Applied Catalysis B: Environmental 201 (2017) 430–437

Contents lists available at ScienceDirect

Applied Catalysis B: Environmental

journal homepage: www.elsevier.com/locate/apcatb

High-surface-area ceria prepared by ALD on Al_2O_3 support

Tzia Ming Onn[a,*], Shuyi Zhang[b,c], Lisandra Arroyo-Ramirez[a], Ye Xia[a], Cong Wang[a], Xiaoqing Pan[b,d], George W. Graham[b,c], Raymond J. Gorte[a]

[a] *Department of Chemical and Biomolecular Engineering, University of Pennsylvania, 34th Street, Philadelphia, PA 19104, USA*
[b] *Department of Chemical Engineering and Materials Science, University of California—Irvine, Irvine, CA 92697, USA*
[c] *Department of Materials Science and Engineering, University of Michigan, Ann Arbor, MI 48109, USA*
[d] *Department of Physics and Astronomy, University of California—Irvine, Irvine, CA 92697, USA*

ARTICLE INFO

Article history:
Received 12 July 2016
Received in revised form 16 August 2016
Accepted 22 August 2016
Available online 24 August 2016

Keywords:
Ceria
Thermal stability
Atomic layer deposition
Palladium
Water gas shift reaction
Redox properties

ABSTRACT

Al_2O_3 powders were modified by Atomic Layer Deposition (ALD) of CeO_2 to produce composite catalyst supports for Pd. The weight of the support was found to increase linearly with the number of ALD cycles. This, together with TEM images, indicated that the CeO_2 grows as a dense, conformal film, with a growth rate of 0.02 nm per cycle. The films showed good thermal stability under oxidizing conditions. XRD measurements on a sample with 0.28 g CeO_2/g Al_2O_3 showed no evidence for crystalline CeO_2 until calcination above 1073 K. Water-gas-shift rates on 1-wt% Pd catalysts supported on the CeO_2 ALD-modified Al_2O_3 were essentially identical to rates on conventional Pd-CeO_2 catalysts and much higher than rates on a catalyst in which Pd was supported on Al_2O_3 with CeO_2 added by infiltration. The WGS rates, together with results from FTIR and CO-O_2 pulse studies, suggest that all of the Pd is in contact with CeO_2 on the ALD-prepared supports and that it should be possible to prepare high-surface-area, functional supports using ALD.

Published by Elsevier B.V.

1. Introduction

The ability of ceria to undergo facile oxidation and reduction makes it effective as an Oxygen Storage Capacitor (OSC) in automotive, three-way catalysts [1–7]. The redox properties are also responsible for promotion of rates on ceria-supported metals for the CO-oxidation [8], water-gas-shift [9–12], methane-steam-reforming [13,14], and methane-oxidation [15] reactions. For CO oxidation, the rate enhancements were shown to depend on the interfacial contact between the ceria and the metal [16], implying that direct contact between the two phases is essential. Unfortunately, the stability of ceria is a problem. In automotive applications, ceria readily crystallizes and sinters, "with growth of particles and loss of surface area, leading to rapid reduction of the oxygen storage and release properties" [17]. Hydrothermal aging and the resulting increase in ceria crystallinity have also been shown to change the thermodynamics of CeO_2 reduction, increasing the magnitude of the heat of oxidation by as much as 50% [18].

Various strategies are used to stabilize the ceria component. First, the OSC component in three-way catalysts is always in the form of a CeO_2-ZrO_2 mixed oxide [19]. These mixed oxides still lose most of their surface area after thermal treatments [20] but the mixed oxides remain thermodynamically reducible. The heats of oxidation for CeO_2-ZrO_2 mixed oxides do not significantly change with particle size or surface area [21,22]. However, a high surface area for the ceria component is still important for maintaining contact with the transition metal. One strategy to stabilize the surface area of the OSC component involves incorporating alumina particles as diffusion barriers to prevent contact between adjacent CeO_2-ZrO_2 particles [17]. This approach has been shown to be effective in maintaining surface areas but introduces difficulties in that the supported metals may not be in contact with the ceria-containing component.

In the present work, we set out to synthesize a composite support of ceria on high-surface-area Al_2O_3 using Atomic Layer Deposition (ALD). While conventional infiltration of Al_2O_3 with $Ce(NO_3)_3$ solutions, followed by heating to decompose the nitrate ions, forms CeO_2 crystallites that cover only a fraction of the surface, ALD is in principle capable of forming uniform, atomic-scale films that cover the entire Al_2O_3 surface. This morphology maximizes the interfacial contact between ceria and any metal catalyst that is introduced to the support. The Al_2O_3 could also stabilize the ceria surface area and prevent crystallite growth, depending on the relative interfacial energies between CeO_2 and Al_2O_3.

* Corresponding author.
E-mail address: tonn@seas.upenn.edu (T.M. Onn).

http://dx.doi.org/10.1016/j.apcatb.2016.08.054
0926-3373/Published by Elsevier B.V.

ALD is a self-limiting process in which films are produced through repeated cycles of reaction between an organometallic precursor and the substrate of interest, followed by oxidation. Reaction of the precursor with the surface is carried out under conditions which limit the reaction to one monolayer, so that the thickness of the final oxide film can be precisely controlled and determined by the number of cycles. Although ALD has found application primarily for fabrication of semiconductor devices, it has also been used in the synthesis of heterogeneous catalysts. For example, ALD has been used to prepare well-dispersed metal particles [23–25] and to stabilize supported-metal particles by "over" coating with an inert oxide film [26–28]. Review papers on the application of ALD to heterogeneous catalysis are available [29–31]. The main issue with using ALD in catalyst preparation is that there can be diffusional limitations with the organometallic precursor when the films are deposited on high-surface-area supports; however, previous work has shown that this can be prevented by using long exposure times in a static system [32,33].

In this paper, we will demonstrate that it is possible to prepare a CeO_2/Al_2O_3 composite support in which CeO_2 exists as a thin film on top of the Al_2O_3. We will also show that this composite support has similar catalytic properties to what would be expected for a high-surface-area CeO_2 support, but with better stability.

2. Experimental methods

Atomic Layer Deposition (ALD) of CeO_2 was performed using a deposition system that has been described in detail in previous publications [32,33]. The system consists of several heated chambers for the substrate, the organometallic precursor, and tubing between the substrate and the precursor, all of which could be evacuated to $\sim 10^{-3}$ Torr using a mechanical vacuum pump. High-temperature valves separated the substrate chamber from the precursor chamber and from both the vacuum pump and the oxygen source. After evacuation, the precursor, Tetrakis (2,2,6,6-tetramethyl-3,5-heptanedionato) cerium, ($Ce(TMHD)_4$, Strem Chemicals, Inc.), was heated to 453 K to produce a vapor pressure of approximately 2 Torr. During the deposition cycle, the $Ce(TMHD)_4$ vapor was introduced to the evacuated sample chamber containing approximately 0.5-g Al_2O_3. The alumina substrate was exposed to the precursor vapor at 503 K for 300 s to ensure that the reaction with the surface was complete. Because a previous study showed that the $Ce(TMHD)_4$ precursor may not be completely oxidized at 503 K [34], in the present study, we removed the sample from the ALD system after evacuation and then heated it to 673 K in a muffle furnace for 5 min between exposures to the $Ce(TMHD)_4$ precursor.

The substrate in this study was a γ-Al_2O_3 (Strem Chemicals, Inc.) that had been stabilized by calcining in air to 1173 K for 24 h. The BET surface area after this pretreatment was 130 m^2/g. To characterize film growth during ALD, gravimetric analysis was performed after every 5 ALD cycles. To benchmark the properties of this composite support, catalysts were also prepared using the unmodified Al_2O_3, the same Al_2O_3 with 0.28 g CeO_2/g Al_2O_3 added by infiltration with aqueous solutions of cerium (III) nitrate hexahydrate (10 g, $Ce(NO_3)_3{\cdot}6H_2O$, Sigma Aldrich) (Referred to here as $CeO_2(IMP)/Al_2O_3$.), and a bulk CeO_2 powder. The $CeO_2(IMP)/Al_2O_3$ was calcined to 673 K for 6 h to remove any nitrates. The CeO_2 powder was prepared by precipitating an aqueous solution of $Ce(NO_3)_3{\cdot}6H_2O$ with excess ammonium hydroxide (NH_4OH, Fisher Scientific), as described in a previous publication [32].

All of the 1-wt% Pd catalysts were prepared by incipient wetness using an aqueous solution of tetraaminepalladium(II) nitrate (Sigma Aldrich). The materials were then dried overnight at 333 K and calcined at 773 K in air for 6 h to remove any organics and nitrates. The elemental compositions of the samples were measured by Inductively Coupled Plasma-Optical Emission spectrometry (ICP-OES) performed on a Spectro Genesis spectrometer with a concentric nebulizer. For the ICP-OES measurement, each sample ($\sim$50 mg) was dissolved in a 5 mL solution of Aqua Regia overnight. The solutions were then diluted with a 10 wt.%. HNO_3 solution to the appropriate concentration before the ICP analysis. The Pd dispersions were determined volumetrically using CO adsorption uptakes at room temperature on the reduced catalysts [10]. In this procedure, the samples were first oxidized in 200 Torr O_2 at 673 K and reduced in 200 Torr H_2 at 423 K before measuring CO uptakes. Dispersions were calculated assuming one CO per surface Pd. Sample surface areas were determined from BET isotherms using N_2 adsorption at 78 K. X-Ray Diffraction (XRD) patterns were recorded on a Rigaku Smartlab diffractometer equipped with a Cu Kα source (λ = 0.15416 nm).

Ex-situ scanning transmission electron microscopy (STEM) was performed on powder specimens that had been sonicated in methanol and dropped onto carbon support films on copper TEM grids (Ted Pella, Inc.) for TEM examination. Specimens were examined with a JEOL 3100R05 electron microscope with double spherical aberration-correctors operated at 300 kV in scanning mode.

Steady-state water-gas-shift reaction rates were measured in a 0.25-inch, quartz, tubular reactor as the carrier gas with partial pressures of CO and H_2O both at 25 Torr (3.3%). The total flow rate of He was kept at 60 mL/min. Before testing, each sample was activated by heating the catalysts to 673 K in the reaction mixture before cooling back to the desired reaction temperature. The light-off profile CO-oxidation rates were also determined in the same flow reactor with CO and O_2 being 25 and 12.5 Torr, respectively, and the balance being He. The total flow rate of the gas mixture was maintained at 120 mL min^{-1}. The samples tested for CO oxidation were previously heated to 1073 K in air before testing. The mass of catalyst used in every rate measurement was 0.10 g and the products were analyzed using a gas chromatograph (SRI8610C) equipped with a Hayesep Q column and a TCD detector. All rates in this study were normalized to the mass of the catalyst. Differential conversions were maintained in all cases.

Fourier Transform Infrared (FTIR) spectra were collected on a Mattson Galaxy FTIR with a diffuse-reflectance attachment (Collector II^{TM}) purchased from Spectra-Tech Inc. Spectra were collected at 4 cm^{-1} resolution. The intensities of the spectral features were normalized by making the background peaks between 700 cm^{-1} and 1000 cm^{-1} be identical for all cases.

The transient-pulse experiments were performed using a system that has been described in other publications [35,36]. The system consists of a tubular reactor equipped with computer-controlled solenoid valves to allow step changes in the composition of the inlet gases. Reactant gases were passed over 200-mg samples in a 1/4-inch quartz tube. The reactor effluent was monitored continuously using an online quadrupole mass spectrometer. The total flow rate with He as the carrier gas was kept constant at 25 mL/min, while the concentrations of the reactive component (either CO or O_2) was chosen to be 10% of the total gas stream. Integration of the partial pressures as a function of time allowed accurate determination of the amounts of CO_2 formed during a CO pulse. Prior to taking the pulse data, we first calcined the samples in 10% O_2 at 673 K for 15 min. This was followed by reduction in 10% CO in Helium at 673 K for 10 min and then re-oxidation in 10% O_2 for an additional 15 min. No attempt was made to analyze the shapes of the pulses because coupling between desorption, re-adsorption, reaction, and diffusion does not allow for a unique determination of rate processes in transient experiments of this type.

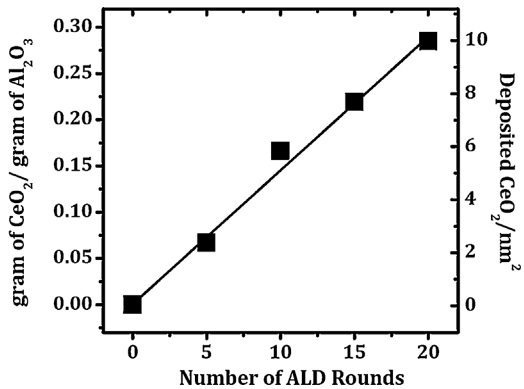

Fig. 1. Mass change as a function of the number of CeO_2 ALD cycles on an Al_2O_3 support which had an initial surface area of 130 m^2/g.

3. Results

3.1. *Characterization of CeO_2 films on Al_2O_3*

The growth rates for the CeO_2 films on Al_2O_3 were determined gravimetrically by measuring the sample mass after every 5 ALD cycles, with results shown in Fig. 1. Similar to what we reported earlier for growth of ZrO_2 films by ALD on a similar alumina substrate, we observed that the sample weight increased linearly with the number of cycles. After 20 cycles, the sample (Referred to here as $20CeO_2$-Al_2O_3) had a total weight gain of approximately 0.28 g CeO_2/g Al_2O_3. That this weight increase corresponded to CeO_2 was confirmed by ICP analysis. Assuming that ceria forms a uniform, dense film with the bulk properties of CeO_2 over the 130-m^2/g Al_2O_3 surface, a 0.28 g CeO_2/g Al_2O_3 loading of CeO_2 corresponds to a film thickness of 0.4 nm ((0.28 g CeO_2/g Al_2O_3) × (1 cm^3/7.21 g CeO_2) × (1 g Al_2O_3/130 m^2) × (1 m^2/10^4 cm^2) × (10^7 nm/cm)). The growth rate calculated from this loading, 0.02 nm/cycle, is identical to the value that has been reported in the literature for this precursor on flat substrates [37] and similar to what was observed previously for ZrO_2 film growth on a similar alumina substrate [32,33].

In order to verify the presence of a thin CeO_2 film, high angle annular dark field (HAADF) STEM imaging was used to characterize the $20CeO_2$-Al_2O_3 sample, as shown in Fig. 2(a) through (d). Due to the atomic number difference between Ce and Al, CeO_2 appears brighter so the surface layer is distinguishable. The images in Fig. 2(a) and (b) were obtained on the fresh sample calcined at 673 K and show that the Al_2O_3 is covered by a relatively uniform CeO_2 film with a thickness close to the expected 0.4-nm. Not surprisingly for deposition on curved surfaces, some slightly larger CeO_2 particles are observed at the higher magnification. The images in Figs. 2(c) and (d) show the same sample after calcination to 1073 K. Under low magnification, Fig. 2(c), the entire surface of the support still appears to be covered with CeO_2. However, small particles, less than 5-nm in size, were also observed at high magnification, Fig. 2(d), along with areas that still show the presence of a CeO_2 film.

The morphology of the $20CeO_2$-Al_2O_3 sample was clearly different from that of the CeO_2(IMP)/Al_2O_3 sample, obtained by infiltration with aqueous solutions $Ce(NO_3)_3$ onto the same Al_2O_3. The images in Figs. 2(e) and (f) were obtained on CeO_2(IMP)/Al_2O_3, which had the same weight loading of CeO_2, after calcination to 673 K. The images show that the CeO_2 exists as 20-nm clusters of roughly 3-nm particles, even after this low calcination temperature. Furthermore, most of the Al_2O_3 remains uncovered by CeO_2. It should be acknowledged that we did not attempt to optimize the impregnation procedure to maximize the CeO_2 dispersion.

Table 1
BET Surface Area as a function of Calcination Temperature. The surface area of the Alumina support is 130 m^2/g.

Calcination Temperature (K)	BET Surface Area (m^2/g)		
	Pd/CeO_2	Pd/$20CeO_2$-Al_2O_3	Pd/CeO_2(IMP)/Al_2O_3
773	42	82	110
973	30	78	100
1073	18	84	100

Table 2
Dispersion Measurement as a function of Calcination Temperature.

Calcination Temperature (K)	Dispersion (%)		
	Pd/CeO_2	Pd/$20CeO_2$-Al_2O_3	Pd/Al_2O_3
773	40	65	34
973	35	63	30
1073	30	59	24

XRD patterns of the $20CeO_2$-Al_2O_3 sample are shown as a function of calcination temperature in Fig. 3, together with the pattern for the untreated Al_2O_3, Fig. 3(a) and the pattern for the CeO_2(IMP)/Al_2O_3 sample, Fig. 3(e). First, it is worth noting that the diffraction pattern of the infiltrated sample with the same CeO_2 loading and calcined to only 673 K, Fig. 3(e), is very different. The peaks associated with CeO_2 dominate on CeO_2(IMP)/Al_2O_3, to the point that the peaks from Al_2O_3 are difficult to see on the same scale due to the larger X-Ray scattering cross section for Ce compared to Al. Even for this relatively low calcination temperature, the CeO_2 domain size, calculated using the Scherrer Equation and the peak width at 28° 2θ, was already 10 nm. By comparison, there is no evidence for the presence of CeO_2 in the $20CeO_2$-Al_2O_3 from the diffraction results after calcination at 873 K, Fig. 3(b). This is consistent with the fact that the domain size for ceria in these samples is very small. Features associated with CeO_2 begin to appear near 28 and 58° 2θ in the diffraction pattern of the sample calcined to 1073 K, Fig. 3(c), and become more prominent after calcination at 1173 K, Fig. 3(d). However, the intensity of the CeO_2 peaks remains weak, implying that much of the CeO_2 is not contributing. Based on diffraction peak widths, the crystallite size of CeO_2 particles was only 8 nm, even after calcination to 1173 K.

3.2. *Catalytic properties*

To determine how modification of the Al_2O_3 support by CeO_2 ALD affects the catalyst-support properties, we examined a series of 1-wt% Pd catalysts prepared from the unmodified Al_2O_3, from the CeO_2 powder, from the CeO_2(IMP)/Al_2O_3 sample, and from the $20CeO_2$-Al_2O_3 sample. It is first interesting to compare the BET surface areas of 1-wt Pd/CeO_2 powder and 1-wt% Pd/$20CeO_2$-Al_2O_3 as a function of calcination temperature. These results are reported in Table 1. Because the γ-Al_2O_3 used here was initially heated to 1173 K, its surface area was only 130 m^2/g. The addition of 20 cycles of CeO_2 by ALD and of 1-wt% Pd by infiltration reduced this to 82 m^2/g. Most of this decrease in specific surface area can be accounted for by the addition of 0.28-g CeO_2 and 0.01-g Pd per gram of catalyst (130 m^2/1.29 g = 100 m^2/g). The additional decrease in specific surface area is likely due to a decreased average pore diameter as the pores of the Al_2O_3 are coated with a nonporous, 0.4-nm film. Calcination of this sample to 1073 K had essentially no effect on the surface area. By contrast, the specific surface area of the Pd/CeO_2 powder decreased from a value of 46 m^2/g after calcination to 673 K, to 42 m^2/g 773 K and 18 m^2/g at 1073 K. Pd dispersion measurements were also performed as a function of calcination temperature on the Pd/Al_2O_3, Pd/CeO_2, and Pd/$20CeO_2$-Al_2O_3 samples, with results shown Table 2. The data indicate that there was

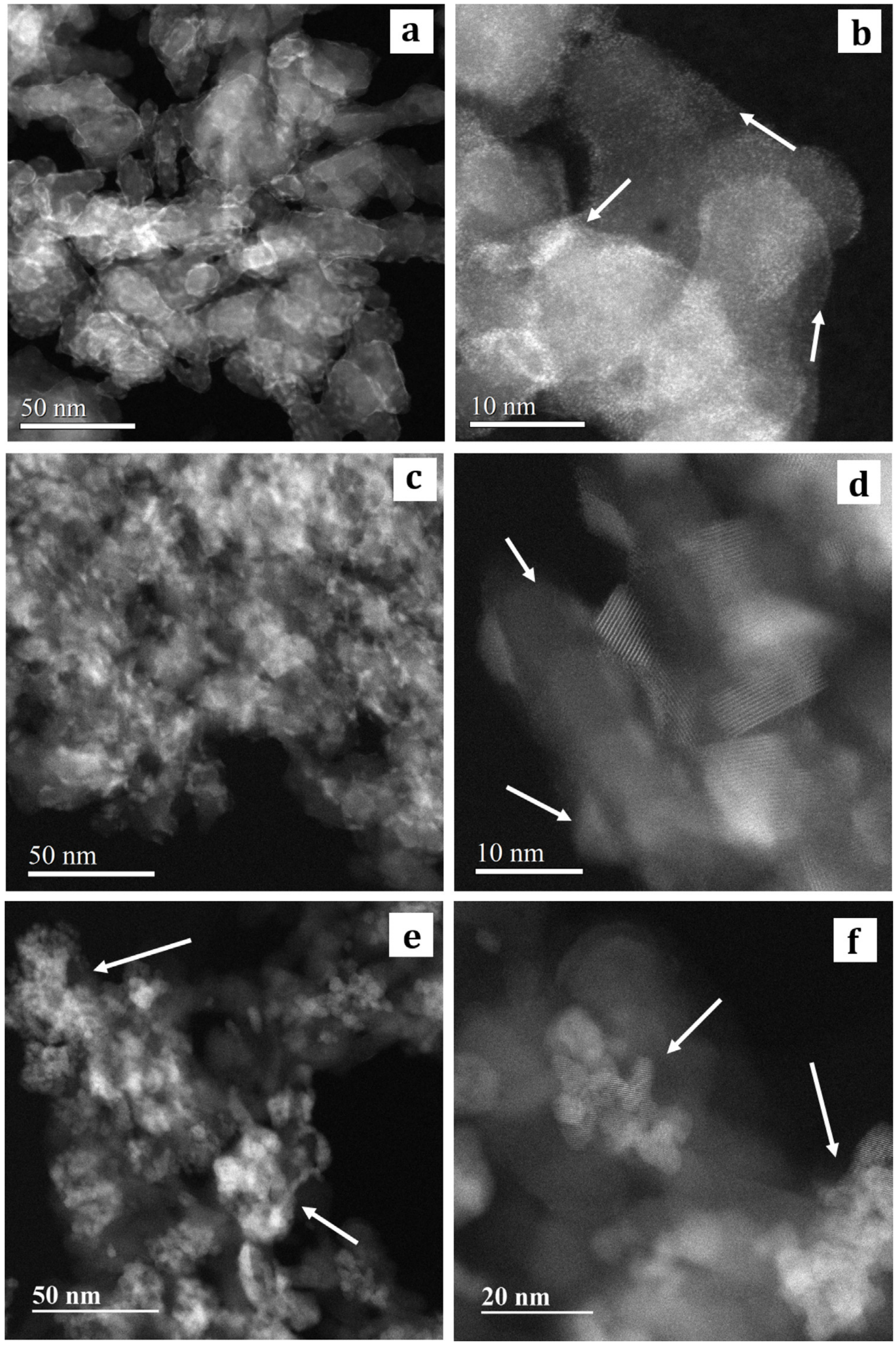

Fig. 2. High angle annular dark field STEM image of ALD $20CeO_2$-Al_2O_3 sample after calcination at 673 K (a–b) and 1073 K (c–d), showing that the uniform atomic CeO_2 layer made through ALD deposition evolved into a mixture of 5-nm CeO_2 particles and CeO_2 film after 1073 K calcination. Impregnated samples after calcination at 673 K (e–f) are shown for comparison. CeO_2 particles appear in agglomerates, ~20-nm in size, and do not cover the surface uniformly. Arrows indicate the location of CeO_2, which appears as the brighter features in all six images.

a fairly significant loss of Pd dispersion with calcination temperature on the Pd/Al_2O_3 sample, from 34% after 773 K and 24% after 1073 K. Given the significant loss in total surface area of Pd/CeO_2, the decrease in dispersion from 40% to 30% in this temperature range is small, indicating that CeO_2 likely helps maintain dispersion [38]. The Pd dispersion on Pd/$20CeO_2$-Al_2O_3 was 65% following catalyst treatment at 773 K and did not change significantly with calcination.

It has been suggested that sites of contact between Pd and ceria are especially active for the WGS reaction due the ability of reduced ceria to be oxidized by water, then transfer either oxygen or OH to CO that is adsorbed on the Pd [9,10]. Based on this picture, WGS rates provide information about whether Pd is in contact with CeO_2 in composite materials. Therefore, differential WGS rates were measured for the Pd/$20CeO_2$-Al_2O_3, Pd/CeO_2, Pd/Al_2O_3 and Pd/CeO_2(IMP)/Al_2O_3 catalysts. The data obtained following calci-

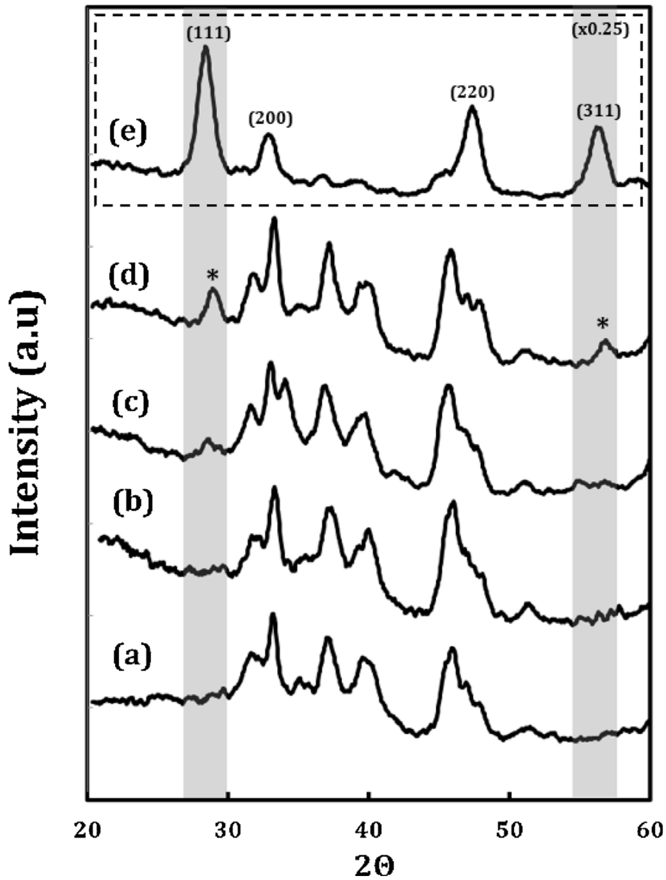

Fig. 3. XRD patterns of the (a) uncoated Al_2O_3 support heated to 1173 K and the ALD-coated, $20CeO_2$-Al_2O_3 sample after calcination to the following temperatures: (b) 873 K; (c) 1073 K; and (d) 1173 K. The pattern in (e) was obtained on CeO_2(IMP)/Al_2O_3 heated to 673 K. Characteristic peaks for CeO_2 are marked by the grey line and *. Peaks were normalized to a distinct Al_2O_3 peak at $2\Theta = 46°$, and the image (e) was scaled by ×0.25.

nation of the catalysts to 773 K are shown in Fig. 4(a). Rates on Pd/CeO_2 were almost 10 times higher than those on Pd/Al_2O_3, as expected. What is more interesting is that the differential rates on Pd/CeO_2 were nearly indistinguishable from rates on $Pd/20CeO_2$-Al_2O_3. Because the ALD-prepared sample is completely covered with CeO_2, its catalytic properties are nearly identical to those of a conventional CeO_2-supported catalyst. Since the Pd dispersions on Pd/CeO_2 and $Pd/20CeO_2$-Al_2O_3 are also reasonably close for 773-K calcination, the number of contact sites between Pd and ceria are also similar. Rates on Pd/CeO_2(IMP)/Al_2O_3 are approximately 2 times lower, probably because some of the Pd particles are not in contact with CeO_2.

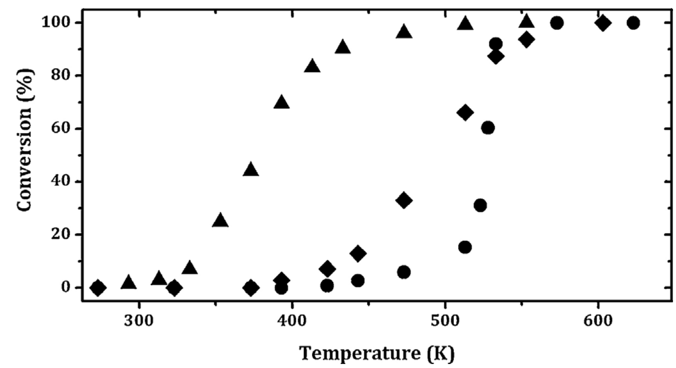

Fig. 5. Light-off curves of CO conversion versus temperature for: (▲) –$Pd/20CeO_2$-Al_2O_3, (♦) –Pd/CeO_2, and (●) –Pd/Al_2O_3 calcined at 1073 K. The CO oxidation reaction was carried out with partial pressures of CO and O_2 at 25 Torr and 12.5 Torr, respectively.

Larger differences in the WGS rates were observed between the samples after the samples were calcined at 1073 K, as shown in Fig. 4(b). Most significantly, rates on the $Pd/20CeO_2$-Al_2O_3 sample remain unchanged. This is consistent with the observations that increased calcination temperature did not affect either the surface area or the Pd dispersion. The fact that the rates remain unchanged implies that contact between Pd and ceria also remains good. Rates on Pd/CeO_2 decreased by a factor of about three after heating to higher temperatures, an amount that is too large to be explained entirely by the lower Pd dispersion. Because loss in ceria surface area is associated with an increase in crystallite size and larger ceria crystallites are considered to be less reducible, it is possible that the decrease in rates is associated with a change in the ceria reducibility. An even larger drop in rates occurs with the Pd/CeO_2(IMP)/Al_2O_3 sample, possibly due to a loss in interfacial contact between the Pd and the ceria component of the support.

To further probe the catalytic properties of these catalysts, we measured light-off rates for CO oxidation on the $Pd/20CeO_2$-Al_2O_3, Pd/CeO_2 and Pd/Al_2O_3 samples after they had been calcined to 1073 K in air. These results are shown in Fig. 5. The light-off tem-

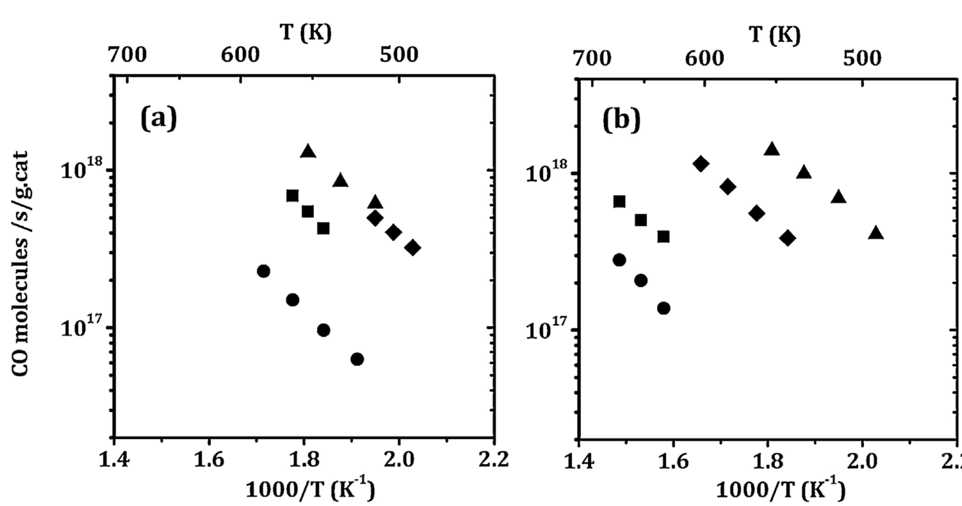

Fig. 4. Steady-state, differential reaction rates for water gas shift (WGS) reaction with partial pressure of CO and H_2O both at 25 Torr. WGS rates after pretreatment calcination to (a) 773 K and (b) 1073 K were compared for the following catalysts: (▲) –$Pd/20CeO_2$-Al_2O_3 (♦) –Pd/CeO_2, (■) Pd/CeO_2 (IMP)/Al_2O_3, and (●) –Pd/Al_2O_3.

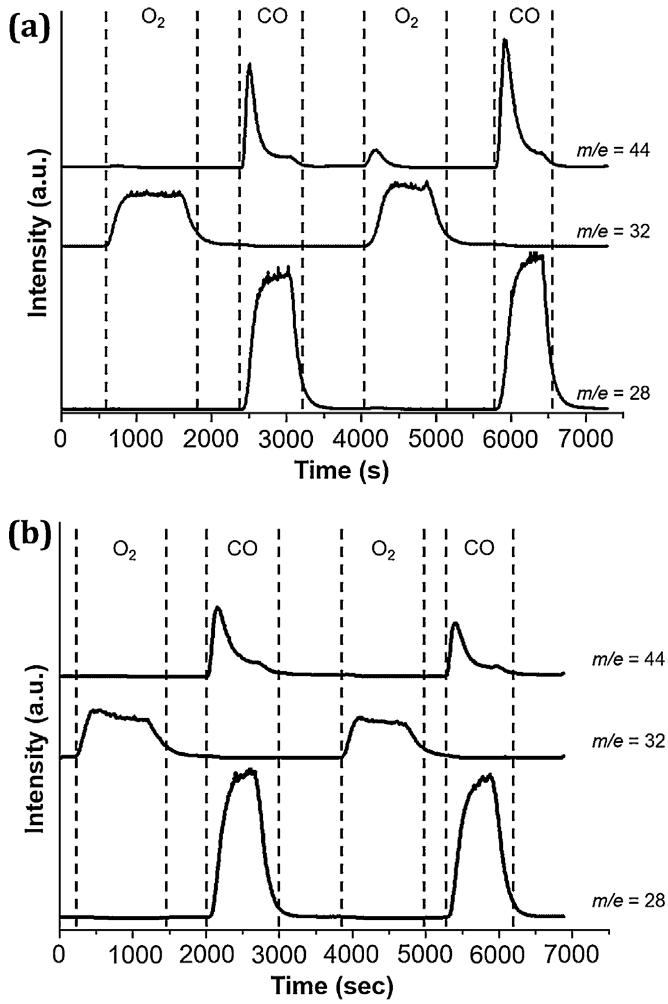

Fig. 6. Pulse measurements on (a) $Pd/20CeO_2$-Al_2O_3, and (b) Pd/Al_2O_3 catalysts at 673 K. The data are for two rounds of CO pulse (m/e = 28) and of O_2 pulse (m/e = 32). Formation of CO_2 (m/e = 44) is observed.

Table 3
Redox data for the pulse-reactor measurements performed at 673 K using CO-O_2 pulses over the samples.

Sample	Average CO_2 (μmol/g) formed from CO pulse
$Pd/20CeO_2$-Al_2O_3	220
Pd/CeO_2	160
Pd/Al_2O_3	87

peratures correspond reasonably well with the relative WGS rates. The $Pd/20CeO_2$-Al_2O_3 sample was by far the most active, followed by the Pd/CeO_2 and Pd/Al_2O_3 samples. Again, the higher rates on $Pd/20CeO_2$-Al_2O_3 are an indication of good contact between Pd and ceria.

The redox properties of $Pd/20CeO_2$-Al_2O_3, Pd/CeO_2 and Pd/Al_2O_3 samples were probed using alternating CO and O_2 pulses at 673 K. Fig. 6 shows a comparison of results for the $Pd/20CeO_2$-Al_2O_3 and Pd/Al_2O_3 catalysts, while a summary of the quantities of oxygen that could be added and removed from the samples is reported in Table 3. In Fig. 6, the regions between the dashed lines correspond to when either 10% O_2 (m/e = 32) or 10% CO (m/e = 28) was added to the He passing over the catalyst. The observation of CO_2 (m/e = 44) upon exposure of the catalyst to CO is due to reduction of the catalyst. Formation of CO_2 during the O_2 pulse on $Pd/20CeO_2$-Al_2O_3, but not on Pd/Al_2O_3, sample is due to decomposition of carbonates that form on reduced ceria [10]. In the calculation of oxygen capacitance, the CO_2 from both the CO and O_2 pulses were added in determining the capacitance. A sample with 1-wt% Pd can provide 94 μmol/g of atomic oxygen by reduction of PdO. For bulk CeO_2, complete reduction to Ce_2O_3 removes 2900 μmol/g of oxygen. The amounts oxygen removed from the Pd/Al_2O_3 sample, 87 μmol/g of CO_2, are within experimental error of the amount expected. Results for $Pd/20CeO_2$-Al_2O_3 and Pd/CeO_2 were similar, forming 220 and 160 μmol/g of CO_2 respectively. In both cases, the ceria in contact with the Pd must be undergoing oxidation and reduction.

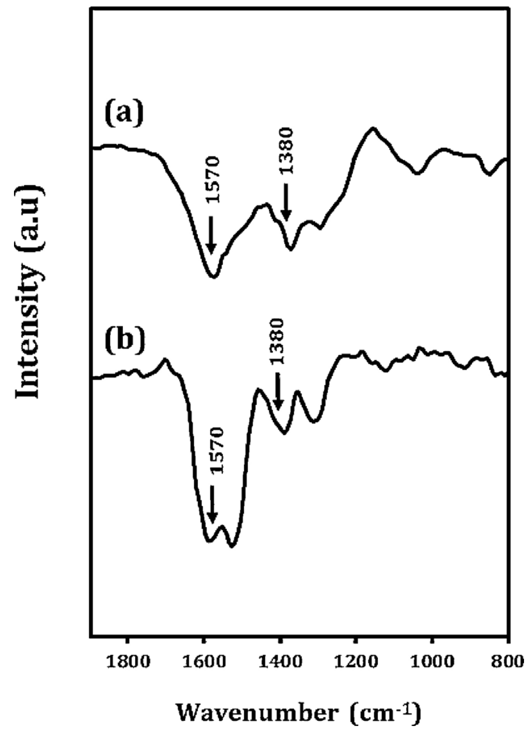

Fig. 7. DRIFTS spectra obtained for (a) Pd/CeO_2 and (b) $Pd/20CeO_2$-Al_2O_3, after exposure to 10% CO in flowing He at 573 K for 10 min.

Finally, in order to compare the surface chemistry of $20CeO_2$-Al_2O_3 and bulk CeO_2, we performed FTIR measurements on the Pd/ceria and $Pd/20CeO_2$-Al_2O_3 catalysts after they had been reduced in 10% CO-He mixtures. As mentioned above, this treatment is expected to reduce the ceria surface and form carbonates. As shown by the spectra in Fig. 7, this is exactly what is observed on both samples. Both samples exhibit broad features between 1300 and 1700 cm^{-1} that correspond to the carbonates. Because absorption in the IR region is strong on bulk CeO_2, the spectrum on $Pd/20CeO_2$-Al_2O_3 is simpler. The results suggest that the ALD-modified sample could be a convenient, model system for spectroscopic characterization.

4. Discussion

The present results indicate that it is possible to prepare a support material with the catalytic, promotional properties of ceria by depositing a thin conformal layer of CeO_2 onto a high-surface-area Al_2O_3 using Atomic Layer Deposition. When used as a support for Pd, the thin CeO_2 film has a similar effect on the water-gas-shift and CO-oxidation reactions as bulk CeO_2. The ALD-modified support has advantages over bulk ceria in that the underlying Al_2O_3 provides surface area for the CeO_2 and stabilizes that area to high-temperature calcination.

The thin-film, CeO_2-coated Al_2O_3 morphology would be difficult to achieve using conventional methods. With normal infiltration

of Ce salts onto Al_2O_3, particles tend to form clusters during the drying or precipitation steps. Similarly, co-precipitation of alumina and ceria will tend to form a mixture of particles in which a large fraction of the surface will be Al_2O_3. As we have seen in the present study, these materials are not as effective as bulk CeO_2, probably because supported metals will distribute between the Al_2O_3 and CeO_2 phases. In this regard, ALD may be unique in providing this hierarchical structure.

The CeO_2 films that were formed by ALD showed surprising good thermal stability upon calcination. Even after calcination to 1173 K, the diffraction peaks for CeO_2 were weak compared to what was observed for a CeO_2/Al_2O_3 formed by infiltration with a similar CeO_2 loading. It is possible that spatial isolation is responsible for maintaining the small crystallites but surface energies may also be responsible. Although CeO_2 does not react with Al_2O_3, Ce^{+3} can form a $CeAlO_3$ perovskite structure. It is therefore possible that there could be bonding interactions at the CeO_2-Al_2O_3 interface. High-temperature reducing conditions could be a problem if compound formation were to occur.

Finally, it is interesting to note that the ALD approach for making "coated" supports is quite general and could be used to make other high-surface-area, functional supports. This opens up a number of opportunities. An obvious extension to the work in this paper would be to prepare CeO_2-ZrO_2, mixed-oxide films. While the mixed oxides are used in today's automotive catalysts, the surface areas are reported to drop below 2 m^2/g [39,40]. Maintaining a higher surface area could enhance the properties of the mixed oxide. In another example, researchers at Daihatsu reported that perovskite-supported catalysts can exhibit very attractive properties [41,42]; however, because most perovskite powders have very low surface areas, it may not be possible to take full advantage of this fact. Preparation of a perovskite film on a support could allow the attractive properties of the perovskite to be used to full advantage.

Clearly, the concept of preparing functional catalysts supports by ALD is still in its infancy. However, we believe this approach could result in catalysts with improved performance and stability.

5. Conclusions

Deposition of CeO_2 by ALD can be used to form thin, conformal films on porous Al_2O_3, and the composites formed in this way can be used as catalyst supports for Pd. The supported-Pd catalysts prepared from the ALD-modified supports exhibit similar water-gas-shift rates to those obtained on conventional Pd/CeO_2 catalysts, implying that there is good contact between the Pd and the CeO_2. The ALD-prepared catalysts have much better thermal stability than conventional CeO_2 supports due to the underlying Al_2O_3.

Acknowledgements

TMO and RJG are grateful to the Department of Energy, Office of Basic Energy Sciences, Chemical Sciences, Geosciences and Biosciences Division, Grant No. DE-FG02-13ER16380 for support of this work. SZ, GG, and XP are grateful to the National Science Foundation, Grant Nos. CBET-1159240 and DMR-0723032 for support of this work.

References

[1] H. Gandhi, G.W. Graham, R.W. McCabe, Automotive exhaust catalysis, J. Catal. 216 (2003) 433–442.
[2] M. Shelef, G.W. Graham, R.W. McCabe, Ceria and other oxygen storage components in automotive catalysts, Catal. Sci. Ser. 2 (2002) 343–372.
[3] R. Di Monte, J. Kašpar, On the role of oxygen storage in three-way catalysis, Top. Catal. 28 (2004) 47–57.
[4] T. Bunluesin, R.J. Gorte, G.W. Graham, CO oxidation for the characterization of reducibility in oxygen storage components of three-way automotive catalysts, Appl. Catal. B: Environ. 14 (1997) 105–115.
[5] J. Kašpar, P. Fornasiero, M. Graziani, Use of CeO_2-based oxides in the three-way catalysis, Catal. Today 50 (1999) 285–298.
[6] R.J. Gorte, Ceria in catalysis: from automotive applications to the water–gas shift reaction, AIChE J. 56 (2010) 1126–1135.
[7] A. Trovarelli, Catalytic properties of ceria and CeO_2-containing materials, Catal. Rev. 38 (1996) 439–520.
[8] T. Bunluesin, E. Putna, R.J. Gorte, A comparison of CO oxidation on ceria-supported Pt, Pd, and Rh, Catal. Lett. 41 (1996) 1–5.
[9] T. Bunluesin, R.J. Gorte, G.W. Graham, Studies of the water-gas-shift reaction on ceria-supported Pt, Pd, and Rh: implications for oxygen-storage properties, Appl. Catal. B: Environ. 15 (1998) 107–114.
[10] X. Wang, R.J. Gorte, J. Wagner, Deactivation mechanisms for Pd/ceria during the water–gas-shift reaction, J. Catal. 212 (2002) 225–230.
[11] C.M. Kalamaras, S. Americanou, A.M. Efstathiou, Redox vs associative formate with–OH group regeneration WGS reaction mechanism on Pt/CeO_2: effect of platinum particle size, J. Catal. 279 (2011) 287–300.
[12] K.C. Petallidou, A.M. Efstathiou, Low-temperature water-gas shift on $Pt/Ce_{1-x}La_x\ O_2{}^-\ \delta$: effect of Ce/La ratio, Appl. Catal. B: Environ. 140 (2013) 333–347.
[13] L. Feio, C. Hori, S. Damyanova, F. Noronha, W. Cassinelli, C. Marques, J. Bueno, The effect of ceria content on the properties of $Pd/CeO_2/Al_2O_3$ catalysts for steam reforming of methane, Appl. Cata. A: Gen. 316 (2007) 107–116.
[14] R. Craciun, W. Daniell, H. Knözinger, The effect of CeO_2 structure on the activity of supported Pd catalysts used for methane steam reforming, Appl. Cata. A: Gen. 230 (2002) 153–168.
[15] M. Cargnello, V.V. Doan-Nguyen, T.R. Gordon, R.E. Diaz, E.A. Stach, R.J. Gorte, P. Fornasiero, C.B. Murray, Control of metal nanocrystal size reveals metal-support interface role for ceria catalysts, Science 341 (2013) 771–773.
[16] M. Cargnello, J.D. Jaén, J.H. Garrido, K. Bakhmutsky, T. Montini, J.C. Gámez, R.J. Gorte, P. Fornasiero, Exceptional activity for methane combustion over modular Pd@ CeO_2 subunits on functionalized Al_2O_3, Science 337 (2012) 713–717.
[17] J.-J. He, C.-X. Wang, T.-T. Zheng, Y.-K. Zhao, Thermally induced deactivation and the corresponding strategies for improving durability in automotive three-way catalysts, Johnson Matthey Technol. Rev. 60 (2016) 196–203.
[18] G. Zhou, P.R. Shah, T. Montini, P. Fornasiero, R.J. Gorte, Oxidation enthalpies for reduction of ceria surfaces, Surf. Sci. 601 (2007) 2512–2519.
[19] T. Montini, M. Melchionna, M. Monai, P. Fornasiero, Fundamentals and catalytic applications of CeO_2-based materials, Chem. Rev. 116 (2016) 5987–6041.
[20] A. Morikawa, T. Suzuki, T. Kanazawa, K. Kikuta, A. Suda, H. Shinjo, A new concept in high performance ceria–zirconia oxygen storage capacity material with Al_2O_3 as a diffusion barrier, Appl. Catal. B: Environ. 78 (2008) 210–221.
[21] P.R. Shah, T. Kim, G. Zhou, P. Fornasiero, R.J. Gorte, Evidence for entropy effects in the reduction of ceria-zirconia solutions, Chem. Mater. 18 (2006) 5363–5369.
[22] T. Kim, J.M. Vohs, R.J. Gorte, Thermodynamic investigation of the redox properties of ceria-zirconia solid solutions, Ind. Eng. Chem. Res. 45 (2006) 5561–5565.
[23] B.S. Lim, A. Rahtu, R.G. Gordon, Atomic layer deposition of transition metals, Nat. Mater. 2 (2003) 749–754.
[24] S.T. Christensen, J.W. Elam, F.A. Rabuffetti, Q. Ma, S.J. Weigand, B. Lee, S. Seifert, P.C. Stair, K.R. Poeppelmeier, M.C. Hersam, Controlled growth of platinum nanoparticles on strontium titanate nanocubes by atomic layer deposition, Small 5 (2009) 750–757.
[25] S.T. Christensen, H. Feng, J.L. Libera, N. Guo, J.T. Miller, P.C. Stair, J.W. Elam, Supported Ru- Pt bimetallic nanoparticle catalysts prepared by atomic layer deposition, Nano Lett. 10 (2010) 3047–3051.
[26] J. Lu, B. Fu, M.C. Kung, G. Xiao, J.W. Elam, H.H. Kung, P.C. Stair, Coking- and sintering-resistant palladium catalysts achieved through atomic layer deposition, Science 335 (2012) 1205–1208.
[27] B.J. O'Neill, D.H. Jackson, A.J. Crisci, C.A. Farberow, F. Shi, A.C. Alba-Rubio, J. Lu, P.J. Dietrich, X. Gu, C.L. Marshall, Stabilization of copper catalysts for liquid-phase reactions by atomic layer deposition, Angew. Chem. 125 (2013) 14053–14057.
[28] T.D. Gould, A. Izar, A.W. Weimer, J.L. Falconer, J.W. Medlin, Stabilizing Ni catalysts by molecular layer deposition for harsh, dry reforming conditions, ACS Catal. 4 (2014) 2714–2717.
[29] S.M. George, Atomic layer deposition: an overview, Chem. Rev. 110 (2009) 111–131.
[30] R.W. Johnson, A. Hultqvist, S.F. Bent, A brief review of atomic layer deposition: from fundamentals to applications, Mater. Today 17 (2014) 236–246.
[31] B.J. O'Neill, D.H. Jackson, J. Lee, C. Canlas, P.C. Stair, C.L. Marshall, J.W. Elam, T.F. Kuech, J.A. Dumesic, G.W. Huber, Catalyst design with atomic layer deposition, ACS Catal. 5 (2015) 1804–1825.
[32] T.M. Onn, S. Zhang, L. Arroyo-Ramirez, Y.-C. Chung, G.W. Graham, X. Pan, R.J. Gorte, Improved thermal stability and methane-oxidation activity of Pd/Al_2O_3 catalysts by atomic layer deposition of ZrO_2, ACS Catal. 5 (2015) 5696–5701.
[33] T.M. Onn, L. Arroyo-Ramirez, M. Monai, T.-S. Oh, M. Talati, P. Fornasiero, R.J. Gorte, M.M. Khader, Modification of Pd/CeO 2 catalyst by atomic layer deposition of ZrO_2, Appl. Catal. B: Environ. 197 (2016) 280–285.
[34] A.S. Yu, R. Küngas, J.M. Vohs, R.J. Gorte, Modification of SOFC cathodes by atomic layer deposition, J. Electrochem. Soc. 160 (2013) F1225–F1231.

[35] S. Sharma, S. Hilaire, J. Vohs, R.J. Gorte, H.-W. Jen, Evidence for oxidation of ceria by CO_2, J. Catal. 190 (2000) 199–204.
[36] T. Luo, R.J. Gorte, Characterization of SO_2-poisoned ceria-zirconia mixed oxides, Appl. Catal. B: Environ. 53 (2004) 77–85.
[37] M. Coll, J. Gazquez, A. Palau, M. Varela, X. Obradors, T. Puig, Low temperature epitaxial oxide ultrathin films and nanostructures by atomic layer deposition, Chem. Mater. 24 (2012) 3732–3737.
[38] J. Jones, H. Xiong, A.T. DeLaRiva, E.J. Peterson, H. Pham, S.R. Challa, G. Qi, S. Oh, M.H. Wiebenga, X.I. Pereira Hernández, Y. Wang, A.K. Datye, Thermally stable single-atom platinum-on-ceria catalysts via atom trapping, Science 353 (2016) 150–154.
[39] R. Voorhoeve, D. Johnson, J. Remeika, P. Gallagher, Perovskite oxides: materials science in catalysis, Science 195 (1977) 827–833.
[40] U.G. Singh, J. Li, J.W. Bennett, A.M. Rappe, R. Seshadri, S.L. Scott, A pd-doped perovskite catalyst, $BaCe_{1-x}Pd_xO_{3-\delta}$, for CO oxidation, J. Catal. 249 (2007) 349–358.
[41] Y. Nishihata, J. Mizuki, T. Akao, H. Tanaka, M. Uenishi, M. Kimura, T. Okamoto, N. Hamada, Self-regeneration of a Pd-perovskite catalyst for automotive emissions control, Nature 418 (2002) 164–167.
[42] H. Tanaka, I. Tan, M. Uenishi, M. Kimura, K. Dohmae, Regeneration of palladium subsequent to solid solution and segregation in a perovskite catalyst: an intelligent catalyst, Top. Catal. 16 (2001) 63–70.